High-Tech Fidget Spinner: Open-Source 3-Axis Turntable

Bhavy Vaibhav Metakar
Hippos Exoskeleton Incorporated
London, United Kingdom
University College London
Electronic and Electrical Engineering
London, United Kingdom
zceebme@ucl.ac.uk

Thomas J. Gilbert
University College London
Electronic and Electrical Engineering
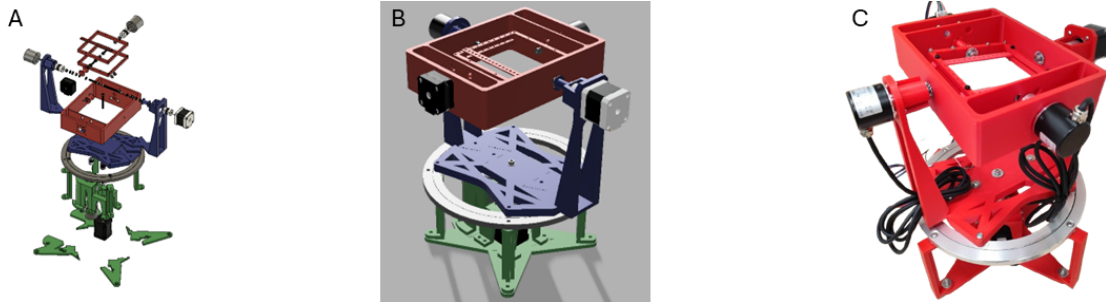London, United Kingdom
thomas.j.gilbert@ucl.ac.uk

Figure 1: 3-DoF IMU-turntable exploded view (A), rendered model (B) and working prototype (C).

Abstract

This paper presents an unprecedented fully open-source, 3-DoF turntable designed to enable precise characterisation and validation of inertial measurement units (IMUs), for under £500, which is a fraction of the cost of commercial systems. This design combines 3D-printed mechanical parts, off-the-shelf 3D printer electronics, and custom firmware with a web-based trajectory generator. Users define piecewise motion profiles for roll, pitch, and yaw via a cross-platform GUI; trajectories are saved to MicroSD and executed on a Teensy 4.1-based controller. The system can achieve a mean deviation as small as $0.0277\,°$ with a resolution of up to $0.0457\,°$, and can hold a wide range of different IMU devices within a $100\,\text{mm} \times 100\,\text{mm}$ area using its universal mounting fixture. All CAD files (STL/3MF/Fusion 360), electronics schematics, firmware source code, and configuration tools are freely available under the GNU GPLv3 license. This platform lowers the barrier to rigorous IMU testing for researchers, educators, and makers without six-figure budgets, which is the cost of commercial solutions.

CCS Concepts

• **Hardware** → *Semi-formal verification*; PCB design and layout.

Keywords

3D Design, Custom Firmware, IMU, Testing, CAD, PCB Design, Webapp UI, Open-Source, FAIR

1 Introduction

Wearable motion tracking systems increasingly rely on inertial measurement units (IMU sensors) to capture biomechanical kinematics live in the field, outside of laboratory settings. As such, IMU sensors are described as a cost-effective alternative to laboratory gold standards [1]. The total addressable market (TAM) for wearables grew by 23.1% from 2020 to 2021, reaching $10.28 billion [21], with 84% of devices used for exploring upper extremity musculoskeletal conditions containing IMU sensors [34].

Conventional IMU validation against optical motion capture systems is prone to marker misalignment, frame rate limitations, and soft tissue artefact (STA) in biomechanical contexts [23], producing a reported error of up to $±42\,°$ using a VR-based system [33]. Mechanical rigs with rotary encoders (turntables) offer a more accurate ground truth with a relative error below 9% [19]. Such IMU turntables are commercially available, but they are costly in the 5 to 6-figure USD range with proprietary firmware as shown in Table 1. This causes inconsistent data comparisons across different studies, and high costs hinder reproducible research.

1.1 Contributions

To address the aforementioned challenges, this paper presents the "High-Tech Fidget Spinner" (the artefact). It is a fully documented, vendor-agnostic and low-cost open-source turntable for IMU characterisation and data validation. This project contributes:

- **Hardware and Mechanical Design:** A modular 3-DoF gimbal, built from 3D-printed PLA and standard 3D printer parts, that executes preset trajectories and universally mounts any IMU device within a 100 mm × 100 mm frame.
- **Electronics and Control:** A control system based on a Teensy 4.1 microcontroller with three TMC2209 drivers and rotary encoders to execute a pre-set trajectory and capture the ground truth.
- **Firmware and Software:** Custom C++ firmware reads binary trajectory files from a MicroSD card, and a Python web app enables intuitive generation of piecewise X/Y/Z profiles.
- **Open Ecosystem:** Full CAD files, BoM, schematics, source code, and documentation released under the GNU GPLv3 license.
- **Validated performance:** Customisable and repeatable rotations about 3 axes with sub-degree precision.

2 Related Work

This section outlines existing commercial closed-source, open-source IMU validation turntables and open-source principles.

2.1 Commercial IMU Validation Rigs

Table 1 shows different DoF, resolution and sample rate specifications for commercial turntables; prices are usually omitted, though the 3LT400 and 13T300 retail in the six-figure USD range. Except for the JAYEGT turntable, they offer at least ≈ 0.001 ° angular resolution and sampling rates from 100 Hz − 1000 Hz.

The JAYEGT turntable is a novelty item, often used for photography. It is not designed to calibrate IMU sensors. Although with such a device, the cost barrier is minimal, it would not be suitable for IMU calibration; Its resolution data and sample rate, amongst other things, are not available.

2.2 DIY and Academic IMU Validation Rigs

There are free plans available on the internet for DIY 1-DoF turntable builds [13, 25, 30], as well as the construction of a simple turntable from an academic project [32].

Some designs available online employ 3D-printed gear mechanisms [13, 25]. Such mechanisms are not suitable for a turntable designed to characterise and validate IMU data due to the non-zero backlash [7].

Other designs [30, 32] employ a direct connection between the rotational actuator shaft and turntable. Two rigidly-coupled rotating shafts eliminate the issue of backlash, but the designs omit rotary encoders for IMU ground truth measurement.

2.3 Open-Source Hardware in Wearables

Open-source hardware should be findable, accessible, interoperable and reproducible [2]. With commercial solutions, they are findable but not accessible due to their cost, not interoperable due to their proprietary firmware and not reproducible due to companies' intellectual property rights. DIY solutions are often findable, accessible, interoperable with modifications and reproducible, but they are not fit for IMU characterisation and validation.

Table 1: Comparison of commercial IMU turntables

Model	Cost / USD	DoF	Resolution / °	Sample Rate / Hz
Firepower Control 3LT400 [28]	210, 000.00	3	0.000833	80
Firepower Control 2TS-450 [5]	NA	2	0.006	1000
Blue Equator BE-INS2-22D08 [10]	NA	2	0.00139	NA
Firepower Control 1LT300 [29]	180, 000.00	1	0.0001	100
iMAR iTES-PDT07 [16]	NA	1	0.00153	NA
iMAR iTURN-2D1-HIL [15]	NA	2	5.56×10^{-6}	1000
iMAR iTURN-3S1 [14]	NA	3	0.0002	1000
JAYEGT Motorized Rotating Display Stand [18]	41.90	1	NA	NA

3 Artefact Overview

This section outlines the design goals for the artefact, the rationale for choosing them and a high-level overview of the system.

3.1 Design Goals

From studying the Related Work, the following design goals were chosen to fill in the gaps identified:

- 3-DoF to outperform some commercial options.
- Synchronous logging of IMU and ground truth data.
- Fully documented and low-cost to be FAIR-compliant [2].
- 360 ° of continuous rotation about all of its axes, to match commercial solutions in Table 1.
- A rotational resolution ≤ 0.05625 ° to surpass the maximum possible resolution by another stepper motor-based turntable [32].
- Bespoke user-defined trajectories for versatility.

3.2 System Architecture

A browser GUI (HTML/CSS/JS frontend, Python/Flask backend) lets users define bespoke piecewise motion profiles and stepper motor parameters. It discretises each axis's trajectory into timed angle steps, saves them to a MicroSD card, and the Teensy 4.1 controller (with TMC2209 drivers) loads and executes them on the X, Y, and
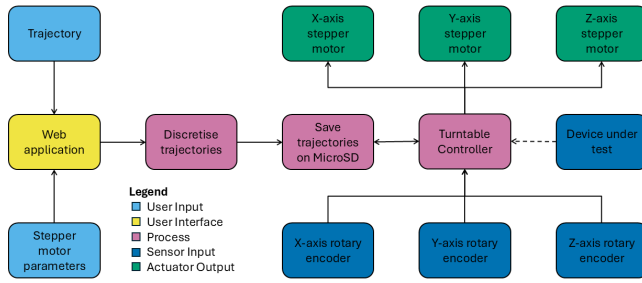
Figure 2: Browser GUI exports users' trajectories as binary files to MicroSD, which the artefact executes.

Z stepper motors. During operation, the controller logs the ground truth via rotary encoders, and IMU data can stream over UART, I2C, or SPI, or be logged separately.

4 Mechanical Design

The artefact consists of a 3-DoF gimbal structure with motor and sensor mounts. The base rotates about the Z-axis. On top of the base, two orthogonal rotating gantries are mounted to rotate about the X and Y axes. A rigid shaft coupling was chosen between the stepper motors and rotating bodies over gearboxes or pulleys to eliminate backlash [7]. Various ball bearings support each frame, constrain a frame's rotation to only its own axis and maintain orthogonal axes.

All rotational frames and brackets were printed in PLA on a Bambulab X1E (0.2 mm layer height, 15 % infill), and the universal fixture clamps in 85A TPU on an Ender 5 (0.2 mm layer height, 20 % infill). Two different 3D printers were used to print the PLA and TPU parts in parallel, as printing in TPU requires a slower print speed and hotter nozzle temperature than PLA [3].

PLA offers higher stiffness (Young's and bending moduli) and impact strength than ABS or PETG. PLA has minimal warp and does not need a heated bed or enclosure, unlike ABS or PETG. [22]. Its low glass transition ($\approx 60\,^\circ$C [22]) limits use to below that temperature but ensures superior rigidity and dimensional stability in that range. PLA prints without enclosures or filtration systems, making it broadly accessible.
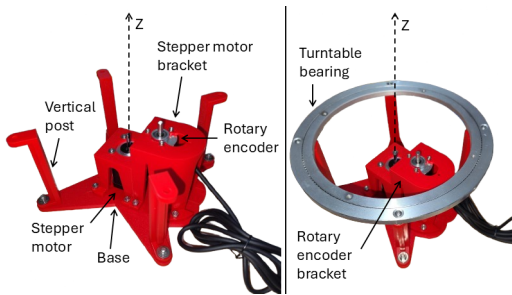
Figure 3: Base frame subassembly (left) for rotation about the Z-axis. A turntable bearing (right) adds stability to the subassemblies mounted on the base.

Figure 3 (left) shows the base subassembly with 4 vertical posts; a bracket for the base stepper motor; a bracket for the base rotary

encoder, and a turntable bearing (right). The bearing mounts on top of the vertical posts to constrain undesired motion [11] for subassemblies on top of the base. The base stepper motor rotates the device under test (DUT) about the Z-axis, and the base rotary encoder measures the rotation about the Z-axis. The rotary encoder is connected to the stepper motor via a GT20 timing belt due to their minimal backlash, as the "backlash is distributed over a full half turn rather than happening immediately on direction change" [27]. Due to practical design considerations of a direct connection between the Z-axis rotary encoder and rotating subassemblies on top of the base, the rotary encoder was driven by a timing belt and pulley system rather than a direct drive.
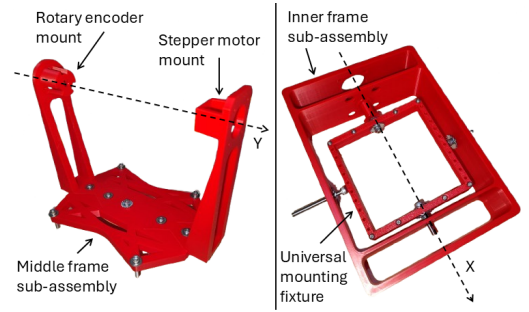

Figure 4: Middle frame subassembly (left) and inner frame subassembly (right) with rotational axes drawn.

Figure 4 (left) shows the middle subassembly with a mount to the turntable bearing on the base; a stepper motor mount, and a rotary encoder mount. It can be mounted to the turntable bearing on the base to ensure stable rotation in the X-Y plane, and a stepper motor and rotary encoder can be mounted along the Y-axis. This allows for rotation about the Y-axis and its measurement.

Figure 4 (right) shows the inner subassembly with a mount for the DUT; a stepper motor mount; a rotary encoder mount, and a mount to the middle assembly. The mount to the middle assembly is a pair of M5 machine screws which attach to the Y-axis stepper motor and rotary encoder through a set of bearings. The inner assembly can be connected to a stepper motor and rotary encoder to rotate the DUT about the X-axis and measure its rotation. The mount for the DUT forms part of the universal mounting fixture, with its other part being 3D-printed out of TPU.

Figure 1C shows the complete mechanical assembly of the artefact with a single point of rotation in the middle of the inner frame about three orthogonal axes. Its cost is under £500 ($\approx$ \$670).
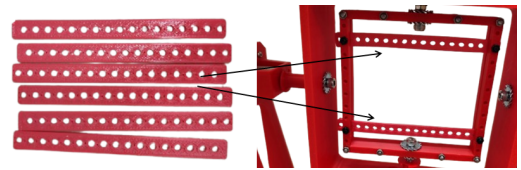
Figure 5: Universal mounting fixture made out of TPU (left) attached to the inner frame (right).

Figure 5 shows the second half of the universal mounting fixture which is 3D-printed out of TPU and attached to the inner frame. The user can configure how many TPU mounts they need, where to place them and their tension using the holes in the TPU mount and the inner frame. The TPU mount is attached to the inner frame using M3 machine screws.
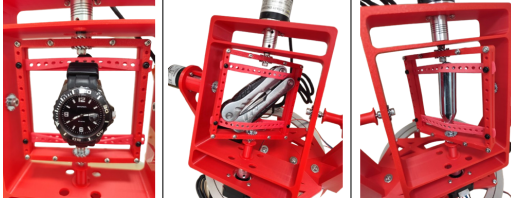
Figure 6: A watch (left), a multitool (middle) and a CO_2 canister (right) secured using the universal mounting fixture.

Figure 6 shows the universal mounting fixture securely holding a watch, a multitool and a CO_2 canister to demonstrate that it can hold a range of different objects, and hence, a range of IMU devices. The user has flexibility over where and how to place their object for their bespoke application.

5 Electronics and Firmware

This section describes the rationale behind the electronic components chosen, shows the schematic and gives an overview of the webapp UI.

5.1 Stepper Motor Selection

5.1.1 Stepper Motors. To achieve 360 ° rotation and ≤ 0.05625 ° resolution on the 3-DoF IMU turntable, open-loop stepper motors were selected for their high native angular precision, simple control and availability [6]. Standard 1.8 ° or 0.9 ° stepper motors (200 or 400 steps per revolution), with up to $\frac{1}{256}$ microstepping, provide a maximum of 0.0035 ° resolution per microstep [4]. Drivers that accept step and direction inputs obviate the complexity of feedback control required for DC or BLDC motors [31].

5.1.2 Dynamic Torque Modelling. Firepower Control's 2TS-450 IMU turntable has an angular acceleration of $300 °s^{-2}$ [5]. To match that lowest commercial angular acceleration from Table 1, each axis was modelled as a compound rigid body composed of cumulative frame, rotor and payload inertias. The model can be found in *./docs/development-log/PRD.md* [26]:

- **X-axis:** $\tau = (2I_{RX} + I_{IMU}) \cdot \alpha$
- **Y-axis:** $\tau = \left(\frac{1}{12}(2M_X + M_{IMU})L^2 + 2I_{RY}\right) \cdot \alpha$
- **Z-axis:** $\tau = \left(\frac{1}{2}(2M_X + 2M_Y + M_{IMU})R^2 + 2I_{RZ}\right) \cdot \alpha$

5.1.3 Selected Motors. A Python script in *./tools/stepper-selection-model/stepper-selection-model.py* [26] was used to select appropriate stepper motors, filtering for those that meet the required torque, size, and inertia constraints with adequate margin and lead time:

- **X-axis:** Nema 17 42-23
- **Y-axis:** Nema 17 42-38
- **Z-axis:** Nema 17 42-60

5.1.4 Microcontroller, Drivers and Rotary Encoders. To maximise versatility, the controller is required to accommodate a user-supplied IMU and allow firmware extension to log data over any digital communication protocol. Commercial IMU turntables in Table 1 employ heterogeneous interfaces (such as CAN bus, which data loggers like laptops lack, and non-uniform USB ports/protocols), and data loggers support varied standards, including CAN bus, SDI-12, and MODBUS. Given the absence of a single, universal logging standard [12], reliance on any one would compromise interoperability; hence, the system must operate autonomously, necessitating on-board storage for recorded data.

Dynamic current control ensures smooth stepper motor performance under varying loads, and support for up to 256 microsteps maximises angular resolution and functional flexibility.

Optical rotary encoders were chosen over magnetic alternatives due to their superior accuracy and resolution [24].

The following components were chosen for the artefact's controller due to their technical specification, cost and lead time:

- **Microcontroller:** Teensy 4.1 due to its 42 assignable GPIOs for UART, I2C and SPI, and a built-in MicroSD card slot [17].
- **Stepper motor driver:** TMC2209 due to its SpreadCycle chopper dynamic current control and 256 microstepping resolution [31].
- **Rotary encoder:** E38S6G5-600B-G24N optical rotary encoder, with 2400 quadrature pulses per rotation (PPR) [8].

5.2 Schematic
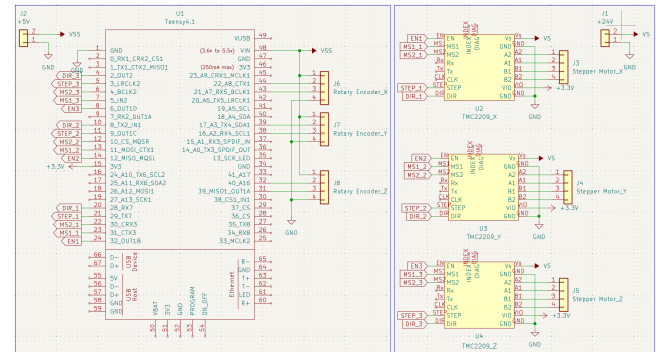
Figure 7: Schematic of the controller for the artefact.

Figure 7 shows the controller schematic consisting of a Teensy 4.1 microcontroller, three TMC2209 drivers, header pin connectors to the stepper motors and rotary encoders. It can be found in *./build/PCB/kicad* [26] and can be constructed on a breadboard with an external power supply (≥ 120 W) for +24 V and +5 V. Files are also provided to manufacture a PCB.

5.3 Code Explanation

The web app GUI shown in Figure 8 allows the user to adjust stepper motor parameters; enter a piecewise trajectory for each axis; display the entered trajectory and discretise the trajectory to be saved onto a MicroSD card for execution by the artefact.
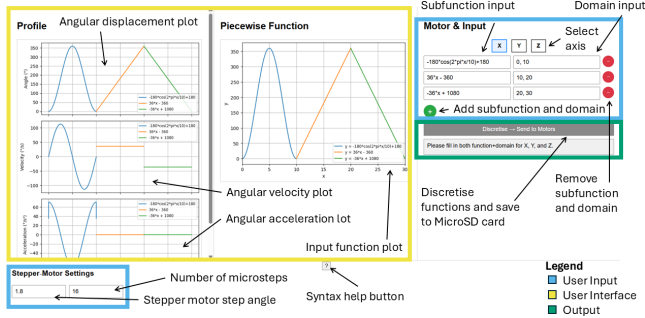
Figure 8: User interface with trajectory input fields (right), and visual trajectories (centre and left).
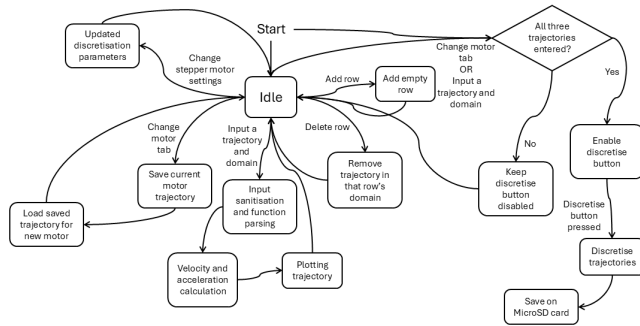
Figure 9: Web application interaction flow diagram.

Figure 9 shows the change between processes due to user inputs. The user can define bespoke trajectories as continuous piecewise functions. The mathematics used to discretise them into executable stepper motor trajectories is as follows:

5.3.1 User Input and Function Parsing. Each motor axis $M \in \{X, Y, Z\}$ accepts a piecewise-defined angular trajectory as a set of symbolic functions $f_i(t)$ defined over domains $[a_i, b_i]$:

$$f_i(t) = \text{sympify}(\text{user input}), \quad f_i^{\text{num}}(t) = \text{lambdify}(f_i(t), \text{numpy})$$

5.3.2 Angular Resolution and Discretisation Step Size. The system computes the angular resolution per microstep:

$$\theta_{\text{res}} = \frac{\theta_{\text{step}}}{\mu}$$

where θ_{step} is the step angle (in degrees) and μ is the number of microsteps.

The angular trajectory is sampled at 1000 uniformly spaced time points; the maximum angular velocity is computed via first-order finite differences:

$$v_{\text{max}} = \max \left| \frac{d\theta}{dt} \right| \approx \max_j \left| \frac{\theta_{j+1} - \theta_j}{t_{j+1} - t_j} \right|$$

The discretisation time step dt is then computed as:

$$dt = \max \left(\frac{\theta_{\text{res}}}{v_{\text{max}}}, \; dt_{\text{min}} \right)$$

where dt_{min} is a fixed lower bound to prevent oversampling (e.g., $dt_{\text{min}} = 0.002$ s).

5.3.3 Sampling and Trajectory Construction. For each segment $f_i^{\text{num}} \in [a_i, b_i]$, we compute the number of samples:

$$N_i = \left\lceil \frac{b_i - a_i}{dt} \right\rceil + 1$$

The time samples are then uniformly spaced:

$$t_j \in \text{linspace}(a_i, b_i, N_i), \quad \theta_j = f_i^{\text{num}}(t_j)$$

The full trajectory is constructed by concatenating all segments while avoiding duplicate boundary points.

5.3.4 Velocity and Acceleration Profiling. Given the discretised angular positions θ_j, the velocity and acceleration profiles are computed numerically via finite differences:

$$\omega_j = \frac{\theta_{j+1} - \theta_j}{dt}$$
$$\alpha_j = \frac{\omega_{j+1} - \omega_j}{dt}$$

5.3.5 Validation and Export. The discretisation process is only enabled once valid input functions and domains are defined for all three axes X, Y, Z. Upon triggering, the discretised trajectories are stored as interleaved binary sequences on a MicroSD card:

$$[\text{uint32 } N][\text{float32 } t_0, \theta_0, t_1, \theta_1, \ldots, t_{N-1}, \theta_{N-1}]$$

6 Evaluation and Benchmarking

This section describes the benchmarking of the presented artefact.

6.1 Method

Infrared reflectors were placed on all rotating frames of the artefact. An Optitrak Prime X 22 motion capture system was used to capture its motion while performing a step trajectory from 0 ° to 90 ° in increments of 10 ° every 2 s. The stepper motor drivers on the artefact were configured to a standard 16-microstep configuration.

The described procedure and its results were from preliminary testing. The community can follow the GitHub [26] for further and more thorough tests after design iterations.

6.2 Results

Figure 10 presents the motion capture measured angular displacement about the X (top), Y (middle), and Z (bottom) axes. Due to the motion-capture coordinate system definition, the measured trajectory rises from 0 ° to 90 ° for the X and Z axes but falls to −90 ° for the Y-axis. Table 2 shows the mean deviation and resolution associated with the data in Figure 10, with the mean deviation and resolution increasing from the X to Z axes due to the greater mass rotating about it, hence, greater inertia and angular momentum.

The maximum sample frequency from the rotary encoders is 100 kHz [8]. It is limited by the artefact's angular velocity, as the output from the rotary encoders is a pulse and the pulse frequency, $f = \omega \times PPR$, where ω is the number of rotations per second and PPR is the number of pulses per rotation.
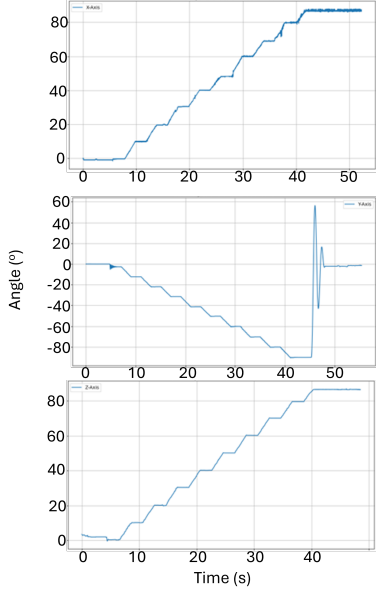
Figure 10: Euler angles of the X-axis (top), Y-axis (middle) and Z-axis (bottom) rotation.

Table 2: Error statistics of the artefact for rotation about each axis

	X-axis	Y-axis	Z-axis
Mean deviation / °	0.0277	0.0287	0.1758
σ (Mean deviation) / °	0.3266	0.8737	0.1603
Resolution / °	0.0461	0.0469	0.0457
σ (Resolution) / °	0.1142	0.0983	0.0586

6.3 Discussion

There were random errors present in the experiment, as the infrared reflectors were manually placed and stuck on using tape. Due to this, there are random errors in marker alignment and since the tape did not create a perfectly rigid joint, the markers underwent harmonic oscillations during acceleration which is shown by the data plotted in Figure 10.

The chosen trajectory was a step trajectory with a linear ramp between each step. This leads to a non-zero starting and ending velocity, and hence, the jolting motion. The largest ranges were observed during harmonic oscillation when the artefact first started moving upon being powered on. The jolting motion due to the trajectory, coupled with the stepper motors jumping to their nearest full steps, is likely the reason behind the largest ranges being one to two orders of magnitude larger than the smallest ranges.

6.4 Future Work

To address the issue of the jolting motion, it would be beneficial to explore how jerk-limited trajectories [20] can reduce the oscillatory motion of the artefact. A closed-loop control system for the stepper motors, such as PID control, remains to be explored for more accurate motions [9]. The maximum angular velocity and acceleration of the artefact have yet to be measured for different payload masses. To reduce random error from motion capture markers taped onto the artefact, the universal TPU mounting fixture can be used to mount the motion tracking markers. Configure the stepper motor drivers to 256 microsteps to increase resolution.

7 Conclusion

As shown by Table 3, the presented artefact demonstrates that IMU characterisation need not be confined to six-figure instrumentation: the fully open-source, High-Tech Fidget Spinner delivers the least angular deviation of 0.0277 ° with the maximum resolution of 0.0457 °, costing under £500 ($\approx$ \$670), and built from readily-available hardware and 3D-printed components. Compared to proprietary, closed commercial systems, it offers versatility and fidelity for a wide class of research, educational, and maker applications to increase access to validation of IMU sensors found in ubiquitous computing devices.

The artefact does not rival the ultimate resolution of commercial turntables, and its maximum velocity, acceleration and payload carrying capacities are unknown. Through community collaboration on the future work, the performance of this High-Tech Fidget Spinner can be further improved. By seeding the community with this accessible infrastructure, there is a possibility for broad adoption, iterative refinement, and novel applications in IMU verification.

Table 3: Comparison of the High-Tech Fidget Spinner to commercial IMU turntables

Turntable	Resolution / °	DoF	Sample Rate / Hz	Openness	Cost / \$
High-Tech Fidget Spinner	< 0.047	3	< 100000	Open	Under 670.00
Firepower Control 3LT400 [28]	0.000833	3	80	Closed	210, 000.00
Firepower Control 1LT300 [29]	0.0001	1	100	Closed	180, 000.00

8 Code Availability

All of the code, supporting files and more details are available at https://github.com/UpsidedownFalcon/IMU-Turntable under the GNU GPLv3 licence [26].

Acknowledgments

References

[1] Jacob S Arlotti, William O Carroll, Youness Afifi, Purva Talegaonkar, Luciano Albuquerque, John E Ball, Harish Chander, Adam Petway, et al. 2022. Benefits of IMU-based wearables in sports medicine: Narrative review. *International Journal of Kinesiology and Sports Science* 10, 1 (2022), 36–43.

[2] Michelle Barker, Neil P Chue Hong, Daniel S Katz, Anna-Lena Lamprecht, Carlos Martinez-Ortiz, Fotis Psomopoulos, Jennifer Harrow, Leyla Jael Castro, Morane Gruenpeter, Paula Andrea Martinez, et al. 2022. Introducing the FAIR Principles for research software. *Scientific Data* 9, 1 (2022), 622.

[3] Emila Brancewicz-Steinmetz, Jacek Sawicki, and Paulina Byczkowska. 2021. The influence of 3D printing parameters on adhesion between polylactic acid (PLA) and thermoplastic polyurethane (TPU). *Materials* 14, 21 (2021), 6464.

[4] Tea Tran Cindy Chang. 2020. *Mastering Precision: Understanding Microstepping in Motion Control.* Retrieved July 9, 2025 from https://www.analog.com/en/resources/analog-dialogue/articles/mastering-precision-understanding-microstepping.html

[5] Firepower Control. 2025. *Remote Control Position Rate Turntable For INS IMU Test And Calibration 2TS-450.* Retrieved July 9, 2025 from https://www.accelerometergyro.com/sale-30377756-remote-control-position-rate-turntable-for-ins-imu-test-and-calibration.html

[6] Clarence W. de Silva. 2005. *Mechatronics: An Integrated Approach.* CRC Press, Boca Raton, FL, USA.

[7] Philipp Eisele, Sajid Nisar, and Franz Haas. 2024. A conceptual examination of an additive manufactured high-ratio coaxial gearbox. *Artificial Life and Robotics* 29, 3 (2024), 416–422.

[8] Sharvi Electronics. 2025. *Datasheet E38S6G5 600B G24N.* Retrieved July 9, 2025 from https://www.scribd.com/document/756625816/Datasheet-E38S6G5-600B-G24N

[9] Nehal M Elsodany, Sohair F Rezeka, and Noman A Maharem. 2011. Adaptive PID control of a stepper motor driving a flexible rotor. *Alexandria Engineering Journal* 50, 2 (2011), 127–136.

[10] Blue Equator. 2021. *High-Precision Automated Dual-Axis Positioning Turntable for INS & IMU Calibration.* Retrieved July 9, 2025 from https://blueequator-ai.com/products/high-precision-automated-dual-axis-positioning-turntable-for-optical-measurement,-aerospace,-and-robotics-calibration

[11] Michael French. 1992. *Form, Structure and Mechanism.* Springer, New York, NY, USA.

[12] Sina Gholamian and Paul AS Ward. 2022. *A Comprehensive Survey of Logging in Software: From Logging Statements Automation to Log Mining and Analysis.* arXiv:2110.12489 doi:10.48550/arXiv.2110.12489

[13] Handy_Bear. 2022. *How to Make a Motorized Lazy Susan With a Secret.* Retrieved July 9, 2025 from https://www.instructables.com/How-to-Make-a-Motorized-Lazy-Susan-With-a-Secret/

[14] iMAR Navigation & Control. 2017. *iMAR iTURN-3S1.* Retrieved July 9, 2025 from https://www.imar-navigation.de/downloads/TURN-3S1.pdf

[15] iMAR Navigation & Control. 2024. *iMAR iTURN-2D1-HIL.* Retrieved July 9, 2025 from https://www.imar-navigation.de/downloads/TURN-2.pdf

[16] iMAR Navigation & Control. 2025. *iTES-PDT-07.* Retrieved July 9, 2025 from https://www.imar-navigation.de/downloads/TES_PDT07_turntable.pdf

[17] Adafruit Industries. n.d.. *PJRC Teensy 4.1 Development Board.* Retrieved July 9, 2025 from https://mm.digikey.com/Volume0/opasdata/d220001/medias/docus/425/4622_Web.pdf

[18] JAYEGT. 2020. *JAYEGT Motorized Rotating Display Stand, 7.87inch /17.6lbs Load, 360 Degree Electric Rotating Turntable for Photography Products, Jewelry, Cake,3D Model ,Mirror Cover (White).* Retrieved July 9, 2025 from https://www.amazon.co.uk/JAYEGT-Motorized-Rotating-Turntable-Photography/dp/B08QS6YTHK

[19] Hua-Kun Jia, Lian-Dong Yu, Hui-Ning Zhao, and Yi-Zhou Jiang. 2019. A new method of angle measurement error analysis of rotary encoders. *Applied Sciences* 9, 16 (2019), 3415.

[20] Hossein Barghi Jond, Vasif V Nabiyev, and Rifat Benveniste. 2016. Trajectory planning using high order polynomials under acceleration constraint. *Journal of Optimization in Industrial Engineering* 10, 21 (2016), 1–6.

[21] Min Jung Kang and Yong Cheol Hwang. 2022. Exploring the factors affecting the continued usage intention of IoT-based healthcare wearable devices using the TAM model. *Sustainability* 14, 19 (2022), 12492.

[22] Shayon Khaled. 2025. *PLA vs ABS vs PETG: The Main Differences.* Retrieved July 9, 2025 from https://all3dp.com/2/pla-vs-abs-vs-petg-differences-compared

[23] Alberto Leardini, Lorenzo Chiari, Ugo Della Croce, and Aurelio Cappozzo. 2005. Human movement analysis using stereophotogrammetry: Part 3. Soft tissue artifact assessment and compensation. *Gait & posture* 21, 2 (2005), 212–225.

[24] Isaac Lara Mekre Mesganaw. 2022. *Differences Between Optical and Magnetic Incremental Encoders.* Retrieved July 9, 2025 from https://www.ti.com/lit/ab/slya061/slya061.pdf?ts=175271104591

[25] MertArduino. 2025. *How to Build a Motorized 3D Scanning Turntable for Your Phone.* Retrieved July 9, 2025 from https://www.instructables.com/How-to-Build-a-Motorized-3D-Scanning-Turntable-for/

[26] Bhavy Metakar. 2025. *IMU-Turntable.* Retrieved August 2, 2025 from https://github.com/UpsidedownFalcon/IMU-Turntable

[27] RepRap. 2015. *Backlash.* Retrieved July 9, 2025 from https://reprap.org/wiki/Backlash

[28] Ltd. Shenzhen Huofeng Technology Co. 2014. *Three-Axis Turntable with Thermal Control for IMU Gyro Accelerometer Sensor.* Retrieved July 9, 2025 from https://shenzhenhuofeng.en.made-in-china.com/product/kfoRCbMGkwWN/China-Three-Axis-Turntable-with-Thermal-Control-for-Imu-Gyro-Accelerometer-Sensor.html

[29] Ltd. Shenzhen Huofeng Technology Co. 2024. *Single-Axis Rotary Rate Position Turntable for Imu Gyro Calibration with Thermal Chamber.* Retrieved July 9, 2025 from https://shenzhenhuofeng.en.made-in-china.com/product/rZKGcOSWwMtd/China-Single-Axis-Rotary-Rate-Position-Turntable-for-Imu-Gyro-Calibration-with-Thermal-Chamber.html?pv_id=1ivd6vdqb9d2&faw_id=1ivd6veb0bc3&bv_id=1ivd704253ac&pbv_id=1ivd6vbrf001

[30] Downeast Thunder. 2020. *DIY Motorized Turntable (FREE PLANS!).* Retrieved July 9, 2025 from https://www.homemadetools.net/forum/diy-motorized-turntable-free-plans-82676

[31] Trinamic. 2023. *TMC2209 Datasheet.* Retrieved July 9, 2025 from https://www.analog.com/media/en/technical-documentation/data-sheets/tmc2209_datasheet_rev1.09.pdf

[32] Eduardo Minuzzi Viera, William D'Andrea Fonseca, and Álysson Raniere Seidel. 2023. *Development of a Turntable for Multidisciplinary Teaching Applications in Electrical, Electronical, and Acoustical Engineering.* Retrieved July 9, 2025 from https://www.researchgate.net/profile/William-Fonseca-4/publication/381485973_Development_of_a_Turntable_for_Multidisciplinary_Teaching_Applications_in_Electrical_Electronical_and_Acoustical_Engineering/links/66710077de777205a335d7dd/Development-of-a-Turntable-for-Multidisciplinary-Teaching-Applications-in-Electrical-Electronical-and-Acoustical-Engineering.pdf

[33] Jan P Vox, Anika Weber, Karen Insa Wolf, Krzysztof Izdebski, Thomas Schüler, Peter König, Frank Wallhoff, and Daniel Friemert. 2021. An evaluation of motion trackers with virtual reality sensor technology in comparison to a marker-based motion capture system based on joint angles for ergonomic risk assessment. *Sensors* 21, 9 (2021), 3145.

[34] Sohrob Milani Zadeh, Joy MacDermid, James Johnson, Trevor B Birmingham, and Erfan Shafiee. 2023. Applications of wearable sensors in upper extremity MSK conditions: a scoping review. *Journal of NeuroEngineering and Rehabilitation* 20, 1 (2023), 158.